Vehicle vibration suppression using an inerter-based mechatronic device

Yujie Shen[a*], Jason Zheng Jiang[b], Simon A. Neild[b], Long Chen[a]
a Research Institute of Automotive Engineering, Jiangsu University, Zhenjiang, 212013, People's Republic of China
b Department of Mechanical Engineering, University of Bristol, Queens Building, University Walk, BS8 1TR, UK
Corresponding author: Yujie Shen E-mail: shenyujie@ujs.edu.cn

Abstract: As a two terminals mechanical element, the inerter has been successfully deployed in various mechanical systems, such as automotives, multi-storey buildings and motorcycles. The introduction of the inerter allows the use of network synthesis to design a passive mechanical network, and can potentially facilitate the identification of practical and high performance mechatronic vibration absorbers. This paper provides an approach for optimal design of both the mechanical and the electrical parts for an inerter-based mechatronic device in vehicle suspension. The system considered includes a mechanical ball-screw inerter alongside an electric motor that isn't driven but instead used passively with an electrical load applied across the terminals. The trade-offs in designing the ball-screw inerter and the permanent magnet electric machinery (PMEM) is discussed in detail. Two factors, namely the coil resistance and the inductor resistance are taken into account in the performance evaluation. Results show that the improvements in the road holding performance can reach 9.24% for the ideal suspension system with no diverse effect on the ride comfort and suspension travel performance, while a 5.77% improvement can be obtained when the effects of the coil resistance and the inductor are included.

Keywords: Vehicle suspension, vibration suppression, mechatronic, inerter, electrical and mechanical network

1. Introduction

As the equivalent to a capacitor under the force-current analogy, a new mechanical network element, the inerter, was first proposed by Smith [1]. It has the feature that the applied force is proportional to the relative acceleration across its terminals. As a two terminal device, it can be included in passive mechanical network synthesis using the 'inerter-spring-damper' networks [2-3]. The inerter has been successfully deployed in Formula One racing [4], and has been proposed for vehicle suspension [5, 6], building vibration suppression devices [7, 8], railway suspensions [9, 10] and landing gear shimmy suppression systems [11]. The mechanical realizations include the ball-screw inerter, the rack and pinion inerter [12], the hydraulic inerter [13] and the fluid inerter [14-16]. For vehicle suspension systems, different suspension layouts employing a passive inerter element was analyzed, and the performance advantages for several different measures were demonstrated compared with conventional passive suspensions [5]. Furthermore, a mechatronic structure consisted of a ball-screw inerter and permanent magnet electric machinery was presented [17], and the performance improvement in a vehicle suspension was demonstrated.

Due to their fast response, good controllability and ability for energy-regeneration, electromagnetic devices can be used in vibration suppression system such as energy harvesting [18] and vibration isolation [19]. By applying an electrical circuit across its terminals, the electromagnetic motor can be considered as a passive device. The electrical network can be considered together with the mechanical network for optimal design. However, the performance of any electromagnetic device may be compromised by its coil resistance, regardless of whether it is used in a small vibration suppression system or in a civil engineering structure. An electromagnetic inerter-based vibration suppression device was proposed, and a power balance analysis was used to ensure the device was self-sufficient [20]. It was pointed out that some of the voltage generated by the electromagnetic device was lost due to the coil resistance, therefore, a voltage compensation unit was deployed to compensate these coil losses. The determined influence of coil resistance was also presented [21], where simulations revealed that almost half the electric energy was dissipated via the coil resistance.

The mechanical and the electrical networks were considered together to improve a vehicle suspension systems performance only based on a specific ball-screw inerter and PMEM [17]. The implications of selecting different types of PMEMs and ball-screw inerter, which might potentially provide enhanced performance, was not discussed. In this paper, a methodology for designing a vehicle suspension structure by using immittance-based solution on the basis of the mechatronic inerter is proposed. To extend the related works, an approach for ball-screw inerter, PMEM and electrical elements' selection are presented here. Some practical factors such as the inductor resistance and coil resistance are also considered in the performance evaluations.

The paper is structured as follows: In Section 2, the mechatronic inerter device, which consists of ball-screw inerter and the permanent magnet electric machinery, is introduced alongside a quarter car model. By considering three performance measurements, a biquadratic function is adopted for the optimal design of the inerter-based vibration suppression device to achieve the goal of improving the vibration isolation performance in Section 3. The trade-offs in designing the ball-screw inerter and the selections of the PMEM are investigated in Section 4. The influences of different motor parameters on the electrical network and on the output performance of the PMEM are also discussed in this part. In Section 5, the vibration suppression performance of the inerter-based mechatronic suspension system is evaluated with the coil resistance and inductor resistance taken into consideration. Conclusions are drawn in Section 6.

2. An inerter-based mechatronic suspension system

2.1 The mechatronic inerter device

The mechatronic inerter consists of ball-screw inerter and rotational permanent magnet electric machinery (PMEM). The schematic of the mechatronic inerter is depicted in Figure 1.

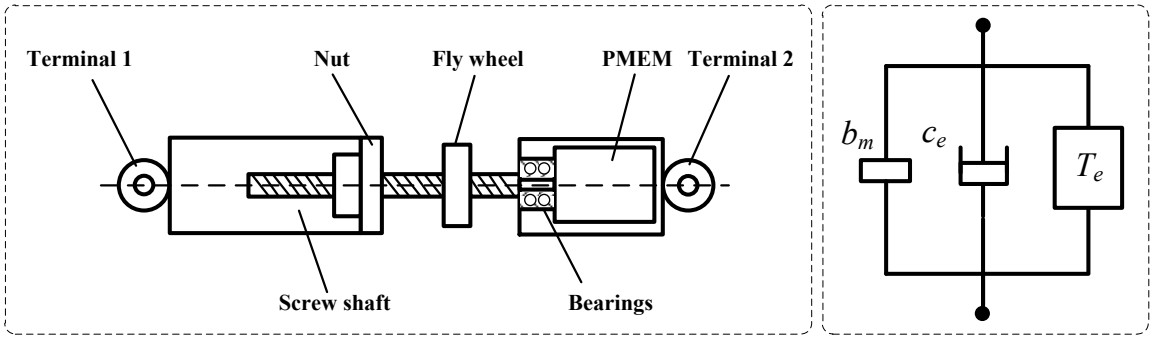

(*a*) Schematic of inerter-based mechatronic suspension

(*b*) Equivalent mechanical network of the inerter-based mechatronic suspension

Figure 1. Schematic of inerter-based mechatronic suspension [17]

where b_m is the mechanical inerter, c_e is the damping coefficient from the toughing parts between the rotor and stator of the PMEM, and T_e represents the electrical part. A PMEM is in series with a screw-shaft rotary type ball-screw inerter. The PMEM rotor will rotate together with the screw-shaft when a force is applied across the terminals of the device. The inertance b_m of the mechatronic inerter can be expressed as

$$b_m = (\frac{2\pi}{P})^2 (J_m + J), \tag{1}$$

where P is the pitch of the ball-screw mechanism, J_m is the mass moment of inertia of the PMEM and J is the mass moment of inertia of the ball screw inerter. The inertance can be supplemented using a flywheel because the mass moment of inertia of the ball screw inerter includes the screw-shaft section and the flywheel section.

2.2 Quarter-car model and performance measures

A standard quarter-car model, shown in Figure 2, with two degrees of freedom is considered. A default traditional suspension structure with a parallel spring and damper layout is taken as a reference. The mechatronic inerter (MI) network is then included in parallel with this traditional suspension structure.

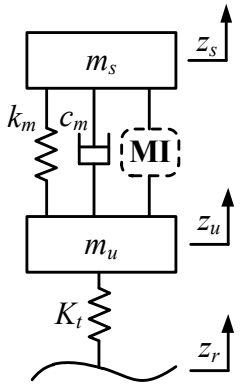

Figure 2. A quarter car model where a mechatronic inerter (MI) network is employed

The dynamic equations of the sprung mass and unsprung mass can be expressed as

$$m_s s^2 Z_s + sT(s)(Z_s - Z_u) = 0, \tag{2}$$

$$m_u s^2 Z_u - sT(s)(Z_s - Z_u) + K_t(Z_u - Z_r) = 0, \tag{3}$$

where Z_s, Z_u and Z_r are the Laplace forms of the vertical displacements of z_s, z_u and z_r respectively. Also, k_m is the stiffness of the spring supporting the vehicle body and c_m represents the mechanical damper's parameter. K_t is the tire stiffness. $T(s)$ is the force to velocity impedance of the suspension system, and can be expressed as

$$T(s) = \frac{k_m}{s} + c_m + T_{MI}(s), \tag{4}$$

where $T_{MI}(s)$ represents the impedance of the mechatronic inerter. Based on Figure 2, the $T_{MI}(s)$ can be expressed as

$$T_{MI}(s) = b_m s + c_e + T_e(s), \tag{5}$$

Note that since the damping coefficient c_e of the PMEM is in parallel in the structure, it can be regarded as supplement in the mechanical damper c_m. When design a vehicle suspension, different performance indexes and constraints are often taken into account simultaneously. For example, the root-mean-square of the body acceleration, and the dynamic tire load, can be used to evaluate the ride comfort performance of passenger and road holding ability, respectively. Meanwhile, the maximum working space of the suspension should be limited to avoid the suspension hitting its end stops [22]. Here, the ride comfort and dynamic tire load [5] will be used as the performance indexes, with the ride comfort J_1 and the dynamic tire load J_3 being expressed as

$$J_1 = 2\pi\sqrt{(Gv)}\left\| sT_{z_r \to z_s} \right\|_2, \quad J_3 = 2\pi\sqrt{(Gv)}\left\| \frac{1}{s} T_{z_r \to K_t(z_u - z_r)} \right\|_2 \tag{6}$$

Here G is the road roughness and v is the forward velocity of the vehicle. If the ride comfort is optimized, the dynamic tire load will be set as a constraint such that its performance meets a default level. In addition we consider the suspension working space as a constraint,

$$J_2 = \left\| \frac{1}{s} T_{z_r \to (z_s - z_u)} \right\|_\infty \tag{7}$$

so that the suspension will not hit its end stop. The parameters are set as v=20 m/s, G=5×10^{-6} m^{3}cycle^{-1}, m_s=320 kg, m_u=45 kg, K_t=190 kN/m, k_m=22 kN/m, c_m=1000 N·s·m^{-1} in this study, which is consistent with the values used by Shen [23]. It can be calculated that for the default traditional suspension using these values $J_{1\text{def}}$=2.6586 m·s^{-2}, $J_{2\text{def}}$=0.3632, and $J_{3\text{def}}$=1816.9 N.

3. Optimal design of an inerter-based mechatronic vehicle suspension

3.1 Identification of beneficial electrical circuits using biquadratic impedances

For the electrical network load $T_e(s)$, a biquadratic transfer function is considered for optimization, which can be expressed as

$$T_e(s) = \frac{As^2 + Bs + C}{Ds^2 + Es + F} \tag{8}$$

Without loss of generality, D can be set to 1 because other parameters can be scaled accordingly. Also, the other parameters' ranges are set as [0, 10^{10}] for optimization. For T_e(s) to be realized by passive electrical networks consisting of resistors, capacitors and inductors, a biquadratic transfer function $T_e(s)$ needs to be positive-real [24]. It has been shown that the positive-real condition for a biquadratic T_e(s) can be expressed as [2]

$$\sigma = BE - (\sqrt{AF} - \sqrt{CD})^2 \geq 0 \tag{9}$$

In the optimization, the cost function will be optimized with the constraint that the other two performance indexes no worse than these of the default passive suspension such that either the ride comfort or the dynamic tire load is optimized with $J_2 \leq J_{2\text{def}}$ and $J_3 \leq J_{3\text{def}}$ or $J_1 \leq J_{1\text{def}}$ and $J_2 \leq J_{2\text{def}}$ respectively. Firstly, the biquadratic transfer function is optimally designed without considering the mechanical inertance and with the k_{m} fixed at the default value of 22 kN/m for a range of damping values. Figure 3 shows the optimized results of the biquadratic transfer function for the different performance criteria. The conventional passive suspension and the constraints are also included to show the comparisons among them. The inset panels present example amplitude bode plots of the transfer function, and a range of [10^{-3}, 10^3] Hz is selected to sufficiently illustrate the representative suspension characteristics of the force to velocity transfer functions.

Figure 3(a) shows that J_1 can be slightly improved from the default value using MI transfer function $T_{MI}(s)$ with b_m set to be 0. With the variation of the damper, three different networks are identified in the optimization. Here, three representative networks with c_m= 750, 1050 and 1250 N·s·m^{-1} are considered. When c_m = 750 N·s·m^{-1}, the network functioned as a damper in the low frequency range, an inerter in the medium frequency, and change to a spring and then a damper in the high frequency. For c_m =1050 N·s·m^{-1}, the network can be regarded as an inerter in the low frequency and a spring in high frequency. Meanwhile, the network acts as an inerter when c_m is 1250 N·s·m^{-1} over the full frequency range.

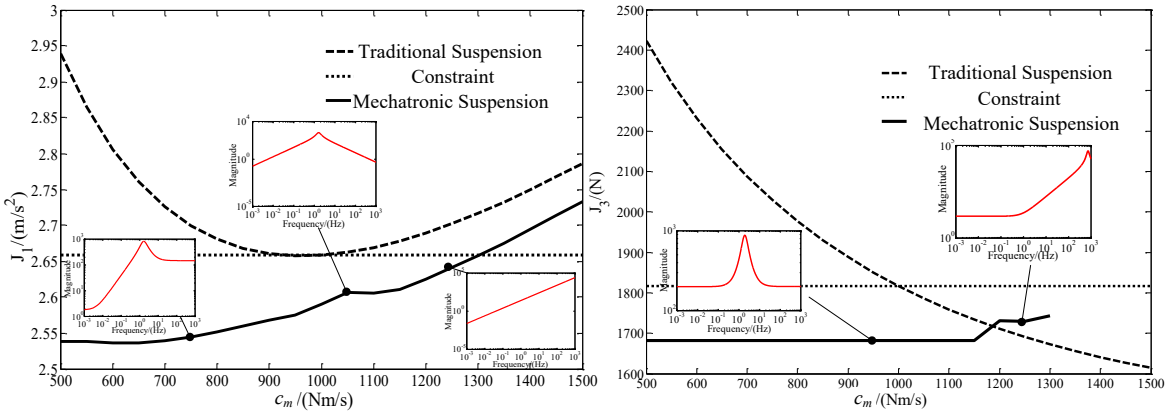

(*a*) Optimization of J_1 using biquadratic transfer function (*b*) Optimization of J_3 using biquadratic transfer function

Figure 3. Optimization of J_1 and J_3 using biquadratic transfer function

Figure 3(*b*) shows the optimization results for J_3.When c_m is larger than 1300 N·s·m^{-1}, there is no optimal solution because the constraint that J_1 is worse than the default suspension cannot be met. Two representative networks are shown when c_m =950 and 1250 N·s·m^{-1}. The first network is more complicated than the second network, because it changes from a damper in low frequency range of [10^{-3}, 10^{-1}] to an inerter around the frequency 1Hz, and then, changes to a spring and finally as a damper in high frequency. The second network is act as a damper in low frequency and an inerter in high frequency.

The biquadratic function can be realized by nine-element networks with three springs, dampers and inerter each using Bott and Duffin synthesis method [25]. It can be checked that all biquadratic functions optimized are 'regular' [2] which mean they can be realized with five-element networks. In order to keep consistent with the dynamic model in Figure 1, the mechanical network representations of these are shown in Figure 4.

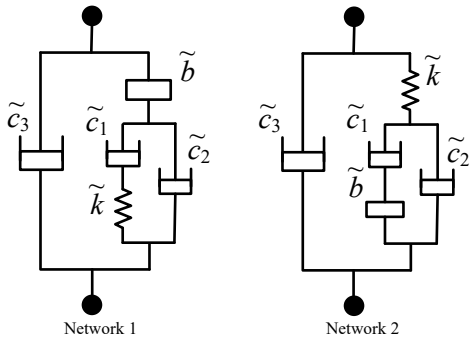

Figure 4. Electrical circuits' layout (mechanical representations)

The detailed parameters of the representative networks are shown in Table 1, and can also be changed to the electrical networks' parameters according the coefficients of the PMEM.

Table 1 Parameters of representative network using the biquadratic function

Objective	Value	c_m(N·s·m^{-1})	Network	$\tilde{k}$(N·m^{-1})	$\tilde{b}$(kg)	$\tilde{c}_1$(N·s·m^{-1})	$\tilde{c}_2$(N·s·m^{-1})	$\tilde{c}_3$(N·s·m^{-1})
J_1(m·s^{-2})	2.5445	750	1	6004.0541	62.8974	942.0259	144.0049	1.7664
	2.6070	1050	1	3046.8491	28.1705	644.5943	3.7946*10^{-6}	8.3721*10^{-9}
	2.6409	1250	1	9.7176*10^{16}	3.8705	2.2829*10^{9}	9.2986*10^{6}	7.1559*10^{-12}
J_3(N)	1681.9	950	1	6140.4826	40.1334	681.0258	0.7904	199.3331
	1729.6	1250	2	5.9332*10^{7}	2.7161	5.1802*10^{4}	15.0029	0.0328

3.2 Optimal design with mechanical inertance b_m

In this sub-section, the inclusion of a mechanical inerter is considered and the electrical load networks are re-

optimized together with b_m. For the networks shown in Figure 4, since $\widetilde{c_3}$ is in parallel with the structure, it can be included in the mechanical damper c_m. When b_m value is selected as 0, 50 and 100kg, J_2 continuously decreases with increasing mechanical damper c_m. Moreover, the value of b_m only has a very weak effect on J_2. For the inerter-based mechatronic vehicle suspension, we impose the restriction that the suspension working space would not exceed its limits by comparing to the traditional suspension system. In the meanwhile, even when the electrical network is not operated, there should be sufficient damping performance in the suppression device. Thus, a mechanical damping in the range [1000, +∞] N·s·m^{-1} is considered in the optimal design. The mechanical damper and inerter alongside with the electrical network are all taken into consideration in the optimization and the optimal results are shown in Table 2. It is noted that, for the suspension 1, $\widetilde{c_1}$ is very large so can be regarded as a rigid connection. According to the results in Table 2, the final inerter-based structures are shown in Figure 5.

Table 2 Parameters of the optimum mechatronic suspension layouts with T_e represented by corresponding equivalent mechanical network

Optimization	k_m (N·m^{-1})	c_m (N·s·m^{-1})	b_m (kg)	$\tilde{k}$ (N·m^{-1})	$\tilde{b}$ (kg)	$\widetilde{c_1}$ (N·s·m^{-1})	$\widetilde{c_2}$ (N·s·m^{-1})	J_1 (m·s^{-2})	J_2 (m)	J_3 (N)	Layout
J_1	22000	1028	5.27	2731.5	28.99	∞	83.99	**2.53**	0.3135	1816.9	1
J_3	22000	1004	2.45	9003.648	96.84	841.14	301.73	2.6586	0.2385	**1649.1**	2

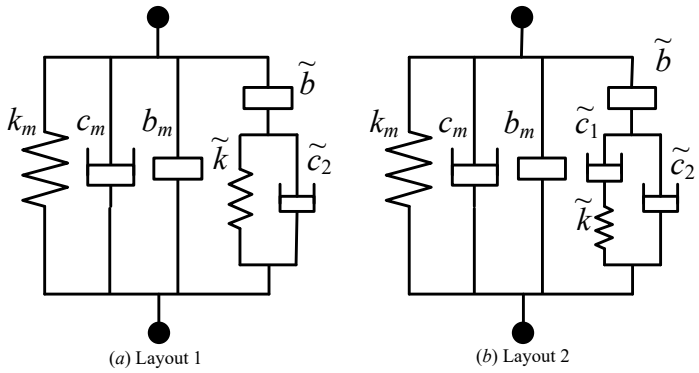

(*a*) Layout 1 (*b*) Layout 2

Figure 5. Mechatronic suspension layouts (with T_e represented by corresponding equivalent mechanical network)

4. Design Trade-offs between the mechanical and electrical parts

In Sections 4 and 5, the optimal results of J_3 will be used as an example to present the detailed approach for designing and analyzing the trade-offs in the ball-screw inerter and the rotational motor of the inerter-based mechatronic vehicle suspension. The inerter-based mechatronic networks shown in Figure 5 can be divided into two parts, namely the mechanical part and electrical part. In the mechanical part, the key point is to design the ball-screw inerter device. Moreover, the corresponding electrical network should be operated within its effective range, for example, within the torque and current limits of the motor, and the voltage and current range for the inductor, capacitor and resistor. In this section, a study of the trade-offs in designing the mechatronic inerter and the PMEM will be discussed.

The inertia of the mechatronic inerter includes two parts: the rotary inertia of the ball-screw inerter and the rotary inertia of the PMEM. In terms of the ball-screw inerter, the inertance relates to the pitch of the ball-screw mechanism, and for the PMEM, the coefficients are essential for the structure design. The characteristic function of the force-velocity behavior of the mechatronic suspension can be shown in Equation (10):

$$Y = (\frac{2\pi}{P})^2[(J_m + J)s + c_e + \frac{k_t k_e}{Z_e(s)}], \tag{10}$$

where c_e is the damping coefficient of the PMEM, k_e is the inductive voltage constant (Vs/rad), k_t is the

inductive torque constant (Nm/A). $Z_e(s)$ is the electrical load impedance. The mechanical inertance can be calculated based on the types of the ball-screw mechanism and the PMEM. For the electrical network, the resistor, inductor and capacitor can be obtained by the following equations:

$$C_e = \frac{\tilde{b}}{K_m},\ R_e = \frac{K_m}{\tilde{c}_e},\ L_e = \frac{K_m}{\tilde{k}_e} \tag{11}$$

where

$$K_m = (\frac{2\pi}{P})^2 k_e k_t \tag{12}$$

Three PMEM are considered in this study with parameters listed in Table 3:

Table 3 Parameters of PMEM

PMEM Type	k_e (Vs/rad)	k_t (Nm/A)	Rated current (A)	Rated torque (Nm)	Coil resistance (Ω)	Rotor Inertia J_m (gcm^2)	Damping Factor (Nm/KRPM)
1	0.0439	0.0438	3	0.09	1.7	155.4	0.001
2	0.0726	0.0724	2	0.10	4	155.4	0.001
3	**0.1098**	**0.1112**	**1.4**	**0.11**	**9**	**155.4**	**0.001**

The ball-screw mechanism is selected according to the datasheet. The standard shaft length is 150mm, the screw shaft inertial moment is 9.99×10^{-6} kg·cm^2/mm. Taking the J_3 optimization results in Table 2 as an example, the variation of the electrical network elements with the change of the pitch value are shown in Figure 6.

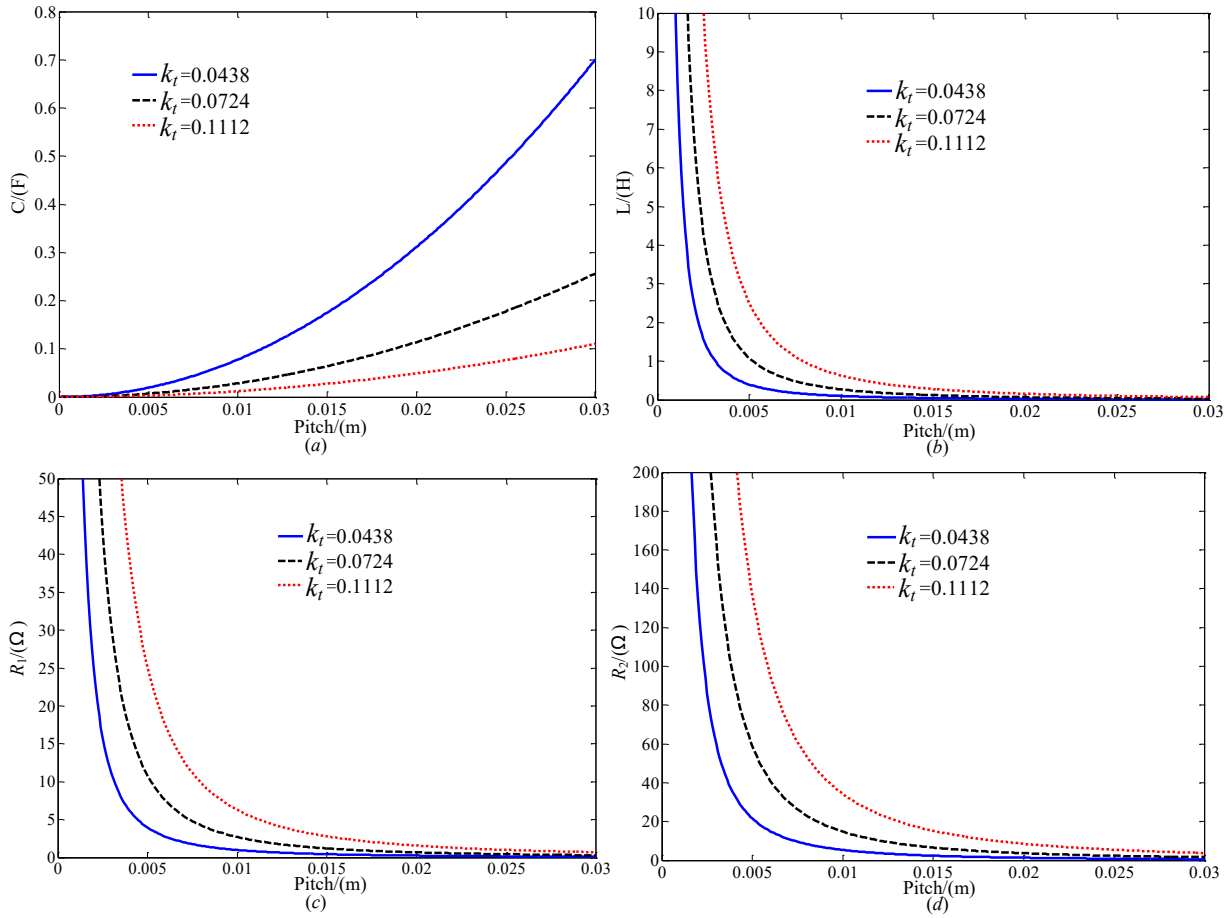

Figure 6. Variation of the electrical elements

The capacitor C, inductor L, resistors R_1 and R_2 are corresponding to the inerter $\tilde{b}$, spring $\tilde{k}$, the damper $\tilde{c_1}$

and $\tilde{c}_2$ of the Layout 2 in Figure 5. It can be seen that, the capacitor value decreases with increasing k_t. However, for a fixed k_t, the capacitor value will become bigger with the increase of pitch value. In contrast, both of the inductor and the resistor values grow with increasing k_t, and become smaller with increasing pitch value.

A time domain response to road roughness input is now taken into consideration. Assuming the vehicle is driving at speed of 25km/h on a grade A road with road roughness is shown in Equation (13) [26]:

$$\dot{Q}_i(t) = -0.111[vQ_i(t) + 40\sqrt{G_q v}w(t)] \tag{13}$$

Here $Q_i(t)$ is the road roughness, G_q=16×10^{-6} is the road roughness coefficient [27], v is the velocity, $w(t)$ is the integral white noise.

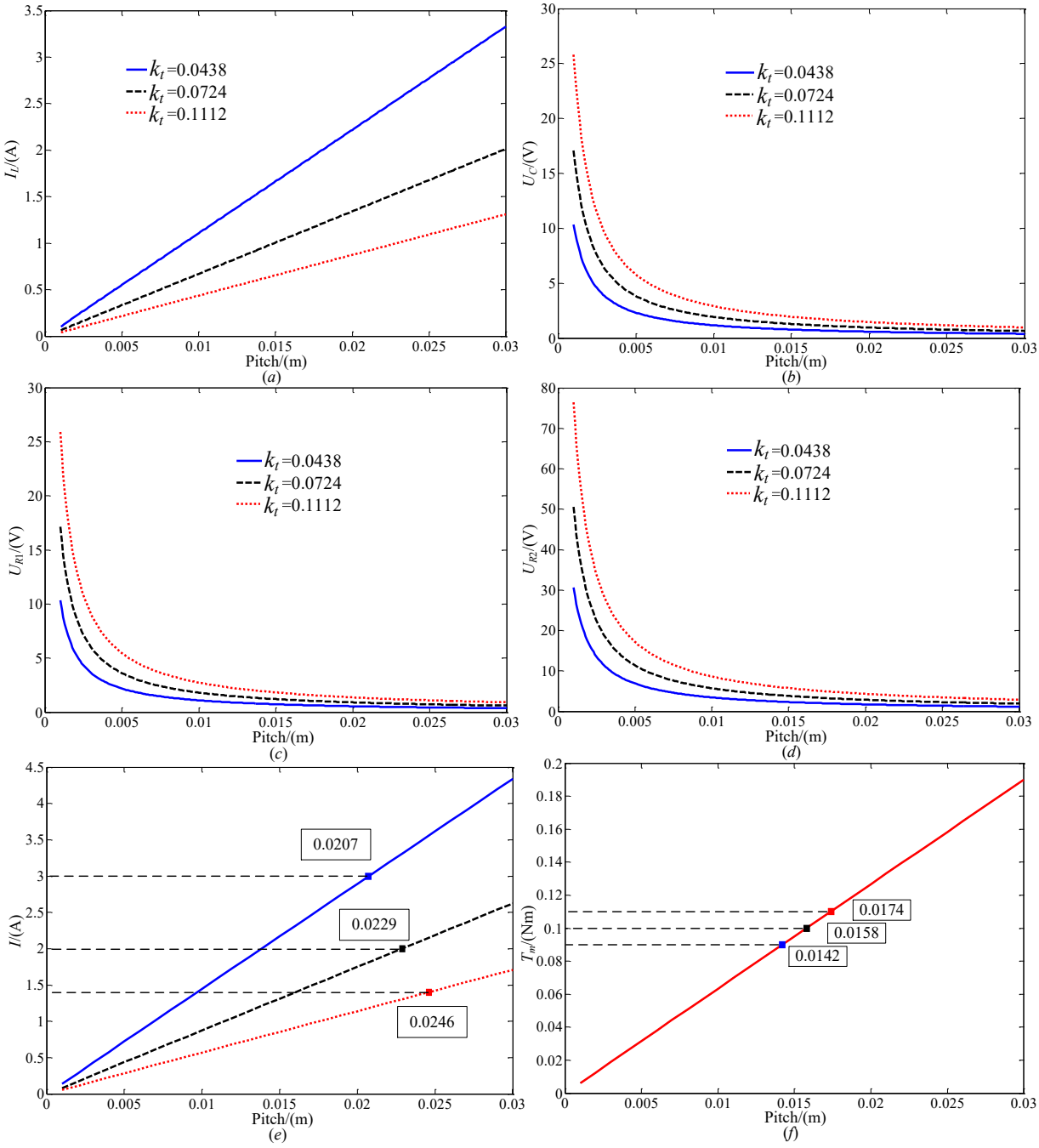

Figure 7. Variations of electrical parameters with the change of ball-screw pitch

Figures 7(*a*) and (*b*) show the variations of the maximum value of the inductor current I_L, capacitor voltage

U_C, Figures 7(*c*) and (*d*) show the variations of resistor voltage U_{R1}, U_{R2}, Figures 7(*e*) and (*f*) show the variations of current in the PMEM I and the torque of the PMEM T_m with the change of ball-screw pitch.

In terms of the capacitor, a maximum voltage must not be exceeded. For the inductor, the current needs to be within a reasonable range to let the inductor work effectively. For the resistors, the working power is used to evaluate the working condition so that the voltage should be limited in a reasonable range. In Figure 7(*a*), (*b*), (*c*) and (*d*), the maximum values are checked across all the pitch variation range, with the maximum current of the inductor I_L under 3.45 A, the maximum voltage of the capacitor U_c under 26V, the maximum voltage of the resistors U_{R1} under 26V and the maximum voltage of U_{R2} under 78V. All of these values are within acceptable ranges according to their datasheet for capacitor, for inductor and for resistors. For the PMEM itself, there is a rated current limitation and a rated torque limitation from Table 3. The current and the torque will continuously increase when the pitch value becomes larger. Thus, an upper boundary of the pitch value can be obtained for the three types of PMEM and marked in Figure 7 (*e*) and (*f*). The upper boundaries of the ball-screw pitch by considering the rated current are 0.0207m, 0.0229m and 0.0246 m. By considering the rated torque, the other upper boundaries can be obtained that, the ball-screw pitch no bigger than 0.0142m, 0.0158m and 0.0174m, respectively.

For J_3 analysis, the optimal mechanical inertance value b_m=2.45 kg in Table 2. By considering the minimum rotor inertia of the ball-screw, is 1.4985×10^{-7} kg/m^2 with no flywheel attached, the rotor inertia of the motor is 1.554×10^{-5} kg/m^2 from Table 3, a lower boundary of the pitch value P_{min}=0.01587m can be obtained according to the equation (1). The selection of the pitch of the ball-screw mechanism should meet the requirements of the available inertance value, the conditional ranges of the current, torque of the PMEM, and the conditional ranges of the current and voltage of the resistor, the inductor and the capacitor. By considering the above factors, a reasonable range of the pitch is [0.01587, 0.0174] m, so that the PMEM type 3 is selected, and the pitch of the ball-screw mechanism is set as 0.016m.

5. Performance analysis

The optimized network is shown in Figure 5(*b*) when analyze the J_3 performance, and the corresponding electrical network can be calculated according Equations (11-12). In actual situation, there is a coil resistor R_m in the PMEM, and an inductor will also have a resistor R_L. The two factors are taken into account in order to analyze the influences on the performance indexes. The actual suspension system is shown in Figure 8. Figure 8(*a*) is the actual mechatronic suspension model involves the mechanical network and the electrical network, and Figure 8(*b*) is the electrical network considering both the coil resistance and the inductor resistance.

Comparing to the ideal mechatronic suspension system, the coil resistor R_m and the inductor resistor R_L using values from the datasheet, are included in the model. The ideal mechatronic suspension and the actual mechatronic suspension considering the coil resistor and inductor are re-optimized for J_3 setting J_1 and J_2 being no worse than the performance of the passive suspension. The results are shown in Table 4. Moreover, Figures 9 shows the magnitudes of the transfer function from the road roughness velocity input to the body acceleration, suspension working space and dynamic tire load.

Table 4 Performance indexes of the different suspension systems

	c_m (N·s·m^{-1})	b_m (kg)	R_1 (Ω)	R_2 (Ω)	C (F)	L (H)	R_m (Ω)	R_L (Ω)	J_1 (m·s^{-2})	J_2 (m)	J_3 (N)
Default traditional suspension	1000	--	--	--	--	--	--	--	2.6586	0.3632	1816.9
Ideal mechatronic suspension	1004	2.45	2.2385	6.2403	0.0514	0.2091	--	--	2.6586	0.2385 (34.33%)	1649 (9.24%)
Actual mechatronic suspension	1150	2.45	0.1319	122.46	0.0232	0.0902	9	4.5116	2.6586	0.2845 (21.67%)	1712 (5.77%)

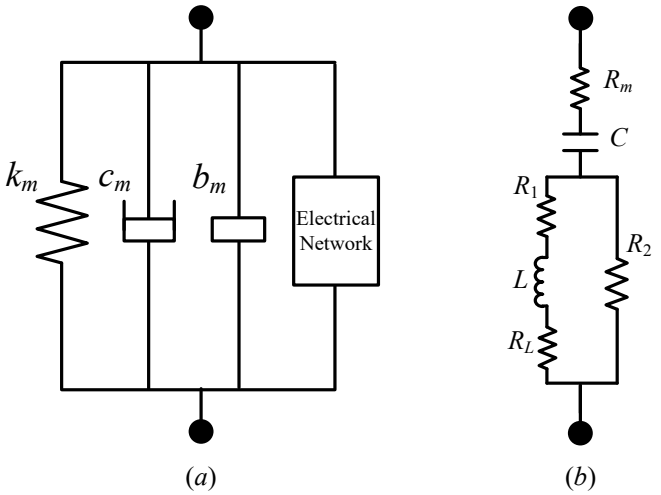

Figure 8. Schematic of the inerter-based mechatronic suspension for optimization of J_3

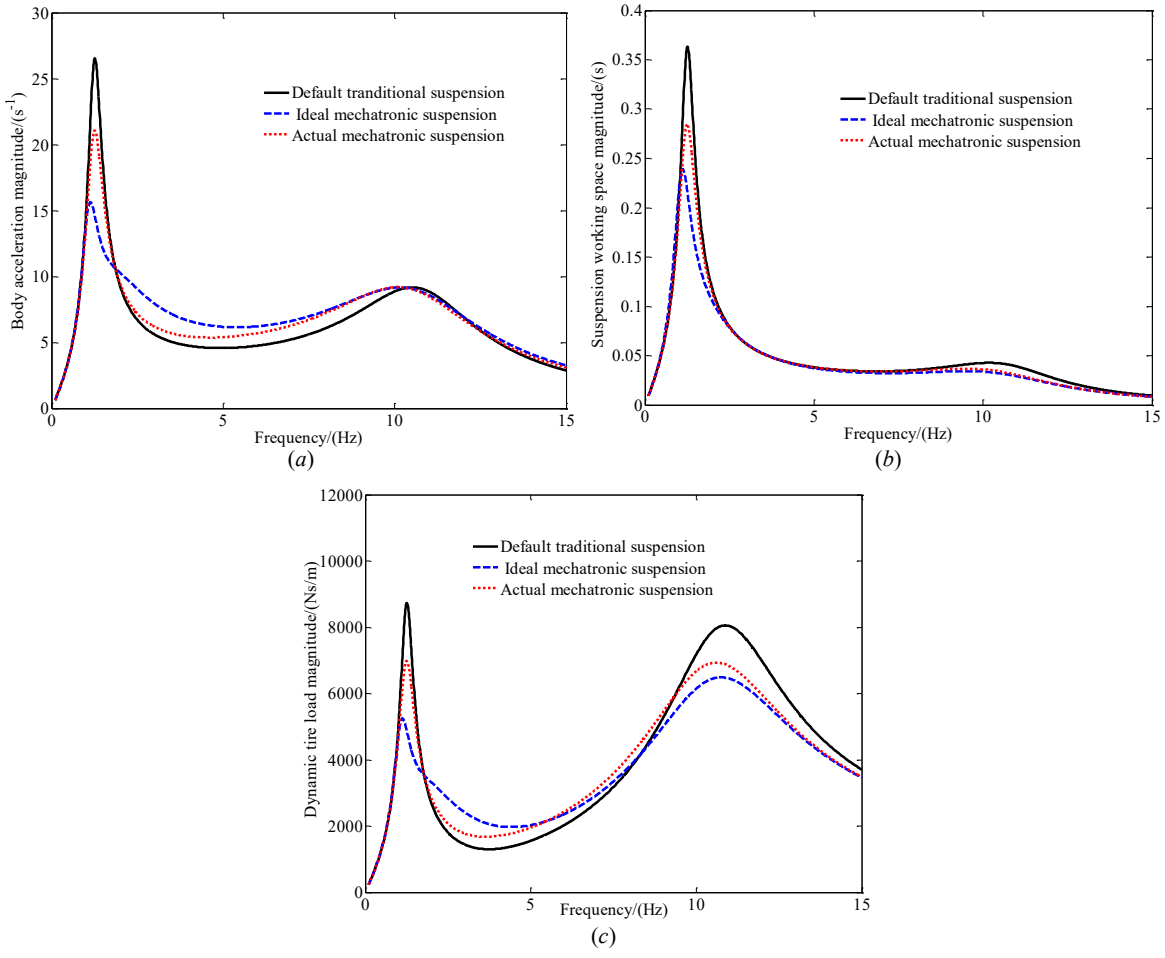

Figure 9. Magnitudes of J_1, J_2 and J_3

It can be seen that, without considering the coil resistance and the inductor resistance, the J_3 index can be improved by 9.24%. At the same time, both the J_1 and J_2 are within the range of the constraints. For J_1, it is the same value of the passive suspension, and there is also a 34.33% improvement for J_2. By considering the R_e and R_L, there will be a performance degradation of J_3, the improvement is decreased from 9.24% to 5.77%. J_1 has the same value as the passive and ideal mechatronic suspension case, J_2 is also affected by the two factors, improvement decreases

from 34.33% to 21.67%. From Figure 9, it is seen that, the resonance magnitude values of the ideal and actual mechatronic suspension in low frequency are significantly decreased, but the magnitudes in middle frequency are increased compared to the default tradition suspension. The improvements are also reduced by considering the R_e and R_L in low frequency, but in middle frequency range, it is converse. For the suspension working space magnitude, both of the ideal and actual mechatronic suspensions' values are less than the default tradition suspension's over the considered frequency, and the magnitude in low frequency is also raised when the R_e and R_L are included. The trends of the dynamic tire load magnitude values are the same with the body acceleration's in low and middle frequency, it the meanwhile, the magnitude values of the ideal and actual mechatronic suspensions in high frequency are also lower than the default tradition suspension.

6. Conclusion

In this paper, an inerter-based mechatronic vehicle suspension for vibration suppression was considered by combining the optimal design of the mechanical and electrical networks. The mechatronic inerter, which involving a ball-screw inerter and PMEM was selected as a basic device, and a standard biquadratic function was included to improve the suspension performance. Using network synthesis, the identified functions were realized using network involving one inerter, one spring and three dampers. Then, the mechatronic inerter was employed in the suspension system, and the optimization was carried out with a limited range of the mechanical damping. The trade-offs in designing the ball-screw inerter and the PMEM were discussed in detail by considering the pitch value and the rated electrical elements working condition. At last, the J_3 optimization was taken as a study case, and the impacts of the coil resistor and the inductor resistor and their impact on the suspension performance were investigated. Results showed that, by using the inerter-based mechatronic vehicle suspension system, the suspension performance can be significantly improved. When the coil resistor and the inductor resistor are taken into consideration, the performance may be degraded. In terms of J_3 results, the improvement may decrease from 9.24% to 5.77%.

Funding

This work was funded by China Postdoctoral Science Foundation (No. 2019M651723) and the China Scholarship Council. S.A.Neild was supported by an Engineering and Physical Sciences Research Council (EPSRC) fellowship (EP/K005375/1). J.Z.Jiang was supported by the EPSRC (EP/P013546/1) and the Royal Society (IE 151194).

Declaration of conflicting interests

The authors declare no conflict of interest in preparing this article.

References

[1] Smith M C. Synthesis of mechanical networks: the inerter. *IEEE Transactions on Automatic Control,* 2002, 47(10): 1648–1662.

[2] Jiang J Z and Smith M C. Regular positive-real functions and five-element network synthesis for electrical and mechanical networks. *IEEE Transactions on Automatic Control* 2011, 56(6): 1275-1290.

[3] Zhang S Y, Jiang J Z, Wang H L, et al. Synthesis of essential-regular bicubic impedances. *International Journal of Circuit Theory and Applications*, 2017, 45(11): 1482-1496.

[4] Chen M Z Q, Papageorgiou C, Scheibe F, et al. The missing mechanical circuit element. *IEEE Circuits and Systems Magazine*, 2009, 9(1): 10-26.

[5] Smith M C and Wang F C. Performance benefits in passive vehicle suspensions employing inerters. *Vehicle System Dynamics*, 2004, 42(4): 235-257.

[6] Hu Y L, Chen M Z Q and Sun Y. Comfort-oriented vehicle suspension design with skyhook inerter configuration. *Journal of Sound and Vibration,*2017, 405: 34-47.

[7] Zhang S Y, Jiang J Z and Neild S. Optimal configurations for a linear vibration suppression device in a multi-storey building. *Structural Control and Health Monitoring,*2017, 24(3): 1887.

[8] Giaralis A and Petrini F. Wind-Induced Vibration Mitigation in Tall Buildings Using the Tuned Mass-Damper-Inerter. *Journal of Structural Engineering,* 2017, 144(2): 8217004.

[9] Wang F C, Liao M K, Liao B H, et al. The performance improvements of train suspension systems with mechanical networks employing inerters. *Vehicle System Dynamics*, 2009, 47(7): 805-830.

[10] Jiang J Z, Matamoros-Sanchez A Z, Goodall R M, et al. Passive suspensions incorporating inerters for railway vehicles. *Vehicle System Dynamics,* 2012, 50(sup1): 263-276.

[11] Li Y, Jiang J Z and Neild S. Inerter-Based Configurations for Main-Landing-Gear Shimmy Suppression. *Journal of Aircraft*, 2016, 54(2): 684-693.

[12] Papageorgiou C and Smith M C. Laboratory experimental testing of inerters. *Proceedings of the 44th IEEE Conference on Decision and Control, and the European Control Conference*, 2005: 3351-3356

[13] Wang F C, Hong M F and Lin T C. Designing and testing a hydraulic inerter. *Proceedings of the Institution of Mechanical Engineers, Part C: Journal of Mechanical Engineering Science*, 2011, 225: 66-72.

[14] Swift S J, Smith M C and Glover A R. Design and modeling of a fluid inerter. *International Journal of Control*, 2013, 86(11): 2035-2051.

[15] Liu X F, Jiang J Z, Titurus B, et al. Model identification methodology for fluid-based inerters. *Mechanical Systems & Signal Processing*, 2018, 106: 479-494.

[16] Shen Y J, Chen L, Liu Y L, et al. Modeling and Optimization of Vehicle Suspension Employing a Nonlinear Fluid Inerter. *Shock and Vibration*, 2016, 5: 1-9.

[17] Wang F C and Chan H A. Vehicle suspensions with a mechatronic network strut. *Vehicle System Dynamics*, 2011, 49(5): 811-830.

[18] Liu Y, Xu L and Zuo L. Design, Modeling, Lab and Field Tests of a Mechanical-motion-rectifier-based Energy Harvester Using a Ball-screw Mechanism. *IEEE/ASME Transactions on Mechatronics*, 2017, 22(5): 1933-1943.

[19] Amati N, Festini A and Tonoli A. Design of electromagnetic shock absorbers for automotive suspensions. *Vehicle System Dynamics*, 2011, 49(12): 1913-1928.

[20] Gonzalez-Buelga A, Clare L R, Neild S A, et al. An electromagnetic inerter-based vibration suppression device. *Smart Materials and Structures*, 2015, 24(5): 055015.

[21] Shi D H, Chen L, Wang R C, et al. Design and experiment study of a semi-active energy-regenerative suspension system. *Smart Materials and Structures*, 2014, 24(1): 015001.

[22] Huang K, Yu F and Zhang Y C. Model predictive controller design for a developed electromagnetic suspension actuator based on experimental data//*Information Engineering (ICIE), 2010 WASE International Conference*, 2010, 4: 152-156.

[23] Shen Y J, Chen L, Yang X F, et al. Improved design of dynamic vibration absorber by using the inerter and its application in vehicle suspension. *Journal of sound and vibration*, 2016, 361: 148-158.

[24] Brune O. Synthesis of a Finite Two-terminal Network whose Driving-point Impedance is a Prescribed Function of Frequency. *Journal of Mathematics & Physics*, 1931, 10(1): 30-36.

[25] Bott R and Duffin R J. Impedance synthesis without use of transformers. *Journal of Applied Physics*, 1949, 20(8): 816.

[26] Sun X Q, Cai Y F, Chen L, et al. Vehicle height and posture control of the electronic air suspension system using the hybrid system approach. *Vehicle System Dynamics*, 2016, 54(3): 328-352.

[27] Yu Z S. *Automotive Theory*, 2011, 203-207